Research Paper

Imparting reusable and SARS-CoV-2 inhibition properties to standard masks through metal-organic nanocoatings

Xiaoling Wang [a,1], Ting Hu [a,1], Bing Hu [b], Yan Liu [c], Yu Wang [a], Yunxiang He [a], Yan Li [d], Kun Cai [b,*], Xingcai Zhang [c,e,**], Junling Guo [a,f,g,***]

[a] BMI Center for Biomass Materials and Nanointerfaces, College of Biomass Science and Engineering, Sichuan University, Chengdu, Sichuan 610065, China
[b] Institute of Health Inspection and Testing, Hubei Provincial Center for Disease Control and Prevention (Hubei CDC), Wuhan, Hubei 430079, China
[c] John A. Paulson School of Engineering and Applied Sciences, Harvard University, Cambridge, MA 02138, United States
[d] Tongji Medical College, Huazhong University of Science and Technology, Wuhan, Hubei 430079, China
[e] School of Engineering, Massachusetts Institute of Technology, Cambridge, MA 02139, United States
[f] State Key Laboratory of Polymer Materials Engineering, Sichuan University, Chengdu, Sichuan 610065, China
[g] Bioproducts Institute, Departments of Chemical and Biological Engineering, Chemistry, and Wood Science, The University of British Columbia, Vancouver, BC, Canada.

HIGHLIGHTS

- R2A mask is prepared with natural biocompatible polyphenol-based R2A nanocoatings showing regeneration ability.
- R2A nanocoatings exhibit high performance on inhibiting SARS-CoV-2 and bacteria.
- R2A mask enables an effectively capture of the aerosols even after 10 recycles.

GRAPHICAL ABSTRACT

ARTICLE INFO

Editor: Danmeng Shuai

ABSTRACT

Face masks are effective response to address this havoc pandemic caused by respiratory infection virus, but they are lack of reusable, antibacterial, and antiviral abilities due to their simple filtration mechanism, bringing to a supply shortage and severe plastic pollution globally. Herein, we designed reusable, antiviral, and antibacterial masks (referred to as R2A masks) that transformed from commonly-used standard masks and household fabrics based on the polyphenol-based surface functionalization. R2A nanocoatings are mainly composed of supramolecular complexation of natural polyphenols and metal ions, possessing a high performance of antibacterial property and comprehensive recyclability. Interfacial interaction of R2A nanocoating can effectively capture the spreading of particulate matters and aerosols containing virus-mimic nanoparticles even after 10 recycles. Moreover, R2A masks exist antibacteria and antivirus for severe acute respiratory syndrome coronavirus 2 (SARS-CoV-2). Collectively, this simple functional enhancement of masks provides a sustainable and strategic preparation for combating the infectious respiratory diseases.

* Corresponding author.
** Corresponding author at: John A. Paulson School of Engineering and Applied Sciences, Harvard University, Cambridge, MA 02138, United States.
*** Corresponding author at: BMI Center for Biomass Materials and Nanointerfaces, College of Biomass Science and Engineering, Sichuan University, Chengdu, Sichuan 610065, China.
E-mail addresses: ckreal@163.com (K. Cai), xingcai@mit.edu (X. Zhang), junling.guo@scu.edu.cn (J. Guo).
[1] These authors equally contributed to this work.

1. Introduction

Coronavirus disease 2019 (COVID-19), caused by the severe acute respiratory syndrome coronavirus 2 (SARS-CoV-2), has grown into a global pandemic. This worst pandemic disease of the current millennium illustrates the key defense strategy of mask against infectious respiratory diseases, which breaks the chain of transmission from person-to-person of direct or close contacting saliva and droplets exhaled from infected people (Howard et al., 2021; Cheng et al., 2021; Wang et al., 2021; Leung et al., 2020a,b; Chu et al., 2020). World Health Organization (WHO) estimated the monthly needs of 89 million medical masks, in additional to the increased and unquantified use of masks by the general public in an attempt to contain the transmission at a global scale (World Health Organization, 2020; Prata et al., 2020; World Wildlife Fund, 2020). A similar utilization worldwide, in 7.8 billion inhabitants, would result in a monthly consumption of 129 billion face masks (Current World Population, 2020).

However, due to the simple mechanical filtration for reducing pathogenic particle transport, the standard mask exists a notable lack of reusable ability (Chua et al., 2020; Brosseau and Ann, 2009). A variety of methods have been developed to address these challenges by engineering advanced masks with the abilities of bacterial and/or viral inactivation through thermal sterilization or generation of reactive oxygen species, including graphene-based masks (Huang et al., 2020a,b; Zhong et al., 2020; Stanford et al., 2019), copper nanoparticles-based masks (Kumar et al., 2020), ionic liquid-polymer-based air filter (Zhang et al., 2020; Chen et al., 2019), and metal-organic framework-based masks (Li et al., 2019). However, from a sustainable perspective, the relatively high cost of material precursors and complex manufacturing processes hamper the large-scale deployment of these techniques in most developing and least developed countries. Currently, the significant increase in production and utilization of masks across the world has given rise to severe challenges to ecosystems and organisms, adding to current burden of 250,000 tons of plastic pollution per day (Fadare and Okoffo, 2020; Ranney et al., 2020; United Nations Environment Programme, 2020). Therefore, there is an urgent need to develop a sustainable strategy of integrating reusability, antiviral, and antibacterial properties to the currently-available standard masks and even household fabrics, while reducing technical difficulties necessary for preparing these materials.

Herein, we explore the use of polyphenol-based surface functionalization to develop a facile and straightforward strategy that transform a range of standard masks and household fabrics (including commonly-used disposable mask, N95 mask, cotton fabrics, and polyester fabrics, Fig. S1 and Table S1, Supporting Information) to a series of reusable, antiviral, and antibacterial masks (referred to as R2A masks) (Fig. 1a–d). The plaque assay and cytopathic effect assay showed that the R2A nanocoatings could effectively inhibit the infection of SARS-CoV-2 on Vero-E6 cells. Moreover, these R2A masks showed a superior rejection performance against the transmission of aerosols containing virus-mimic nanoparticles (100 nm) during a 10-time recycle. In addition, these function-enhanced masks also exhibited stable ~ 99% bacteriostatic rates following 10 cycles and high filtration efficiencies against polluted particulate matters ($PM_{1.0}$, $PM_{2.5}$, and PM_{10}). This facile and easily applicable functional enhancement strategy of masks provides a sustainable development to fight against the currently rapid spread of COVID-19 and newly-discovered viruses in future scenarios.

2. Experimental section

See Supplementary Information for a detailed description of materials, characterizations, aerosol rejection, antibacterial assay, PMs filtration, Figs. S1–S41, and Table S1.

2.1. Preparation of R2A masks

The surfaces of masks and household fabrics can be functionalized based on the use of coordination-based metal-phenolic network (Guo et al., 2018, 2016, 2014; Luo et al., 2019; Ejima et al., 2013; Zhao et al., 2020; Qiu et al., 2021; Li et al., 2021). Briefly, the masks (disposable mask and N95 mask) and household fabrics (cotton and polyester with the size of 170 mm × 90 mm) were sprayed with R2A precursor solution (5.0 mL, containing 6 mmol L^{-1} of tannic acid and 36 mmol L^{-1} of $CuCl_2$) and buffer solution (5.0 mL, pH 7.4, containing 200 mmol L^{-1} of $Na_2HPO_4 \cdot 12 H_2O$ and 100 mmol L^{-1} of $C_6H_8O_7$) in sequence. After 1 min, the R2A masks were washed with Milli-Q water to remove excess complexes and dried naturally. Thus, the R2A nanocoatings were coated on the mask fibers to afford functional R2A masks. After protection, the R2A masks were sprayed with acetic acid solution (10 mL, 5% in Milli-Q water (*v/v*)). The R2A nanocoatings were disassembled with the simultaneously removal of attached particles, bacteria, and virus. Thus, the standard masks and house fabrics can be recovered, which allows the regeneration of R2A masks by re-spraying R2A precursor solution and buffer solution in sequence.

2.2. Cytotoxicity assay of R2A nanocoatings

The effect of R2A nanocoatings on the proliferation of Vero-E6 cells (derived from normal African green monkey kidney) was analyzed using Cell Counting Assay (CCK-8) (Dojindo Molecular Technologies, Inc, Japan). Vero-E6 cells were pre-incubated in a 96-well plate at 37 °C with 5% CO_2 for 24 h. R2A precursor solution (containing 0.6 mg of R2A nanocomplexes) was diluted with DMEM (2% FBS) to four concentration gradients (2, 4, 8, 16 µg mL^{-1}). 100 µL of each gradient was added to Vero-E6 cells and repeated for six times. At the same time, the cell control (without R2A nanocomplexes) was set. All plates were incubated at 37 °C with 5% CO_2 for 1 h and 48 h, respectively. Then, the plates were washed by Hank's solution for twice. After 100 µL of DMEM (2% FBS) was added and incubated for another 48 h, the DMEM was removed. 100 µL of fresh DMEM (2% FBS) and 10 µL of CCK-8 solution were added in sequence. After incubation for 1 h, the absorbance at 450 nm was detected by enzyme reader (Tecan Infinite 200 PRO, Austria).

2.3. Plaque assay

A total of 1×10^6 Vero-E6 cells per well were pre-incubated overnight in a 12-well plate before performing the plaque assay. The culture medium was removed and washed twice with PBS. 100 µL of SARS-CoV-2 strain (WBP-1, 1.58×10^7 TCID50 mL^{-1}) solution and 100 µL of R2A precursor solution (containing 0.6 mg of R2A nanocomplexes) were mixed and incubated at 37 °C for 1 h. Then, the R2A nanocomplexes and virus mixture was diluted 10-fold with DMEM (2% FBS). 500 µL of the appropriate dilution (10^{-1}, 10^{-2}, 10^{-3}, 10^{-4}) was added to the corresponding wells with monolayer Vero-E6 cells. Each gradient was repeated for three times. After incubating for another 1 h (37 °C with 5% CO_2), the mixture solutions were removed and the wells were washed by Hank's solution for twice. 100 µL of DMEM contained 1.8% methyl cellulose (MC) and 2% FBS was added to each well and discarded after incubating for 48 h at 37 °C with 5% CO_2. The Vero-E6 cells were fixed with 10% formalin at least 1 h and stained with 0.2% crystal violet overnight to observe the formation of plaque. The control group (without R2A nanocomplexes) was designed at the same time.

2.4. Cytopathic effect (CPE) assay

SARS-CoV-2 strain (WBP-1, 1.58×10^7 TCID50 mL^{-1}) solution and R2A precursor solution (containing 0.6 mg of R2A nanocomplexes) were mixed at the equal volume and incubated for 1 h. Then, the mixture was diluted 300-fold in DMEM (2% FBS), so that the initial titer of the virus
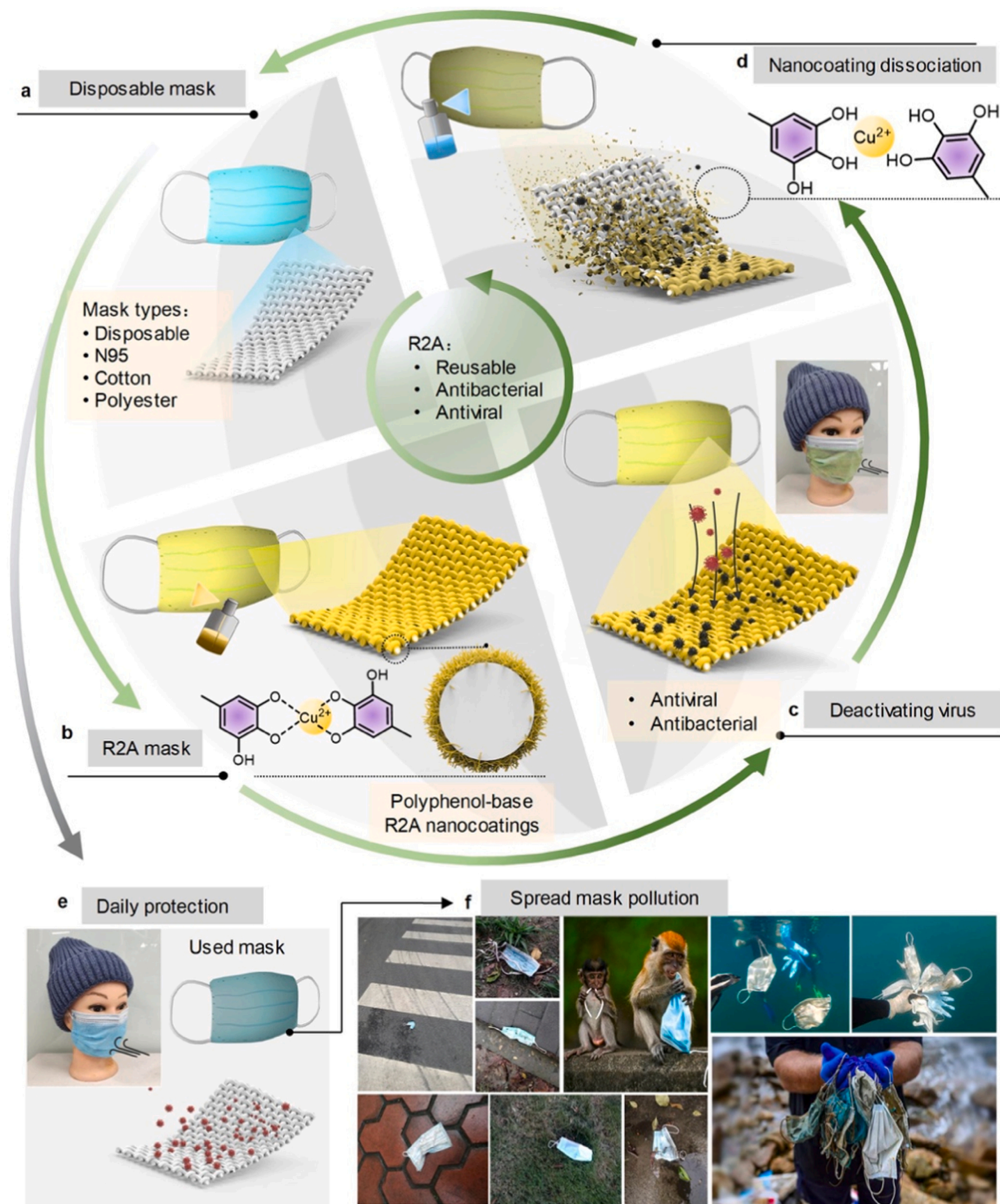
Fig. 1. Schematic of the preparation of R2A mask connected with dynamic metal-phenolic circular chemistry. (a) Available list of the commonly-used masks and household fabrics and their demonstration of functional enhancement. (b) Surface functionalization-based enhancement of masks and the formation of polyphenol-based R2A nanocoatings. (c) Antiviral and antibacterial properties of R2A masks. (d) Schematic illustration of the disassembly of the R2A nanocoatings and removal of deactivated virus, bacteria, and polluted particulate matters. (e) The remaining of living virus and bacteria on the disposable masks causes infectious risks. (f) Representative digital photos of environmental pollutions caused by the disposed masks.

was 5000 TCID50 100 μL^{-1}, which was further diluted to make every mixture gradient contain 1000, 200, 100, 20 TCID50 100 μL^{-1}, respectively. Then, 500 μL of each dilution was added to a 24-well plate with 10^4 Vero-E6 cells per well and incubated at 37 °C with 5% CO_2 for 48 h. The viral titers were repeated for four times. The CPE results of Vero-E6 cells were observed by microscope. The control group (without R2A nanocomplexes) was set at the same time.

All experiments involving living virus were performed in a biosafety level 3 (BSL3) facility in the Institute of Health Inspection and Testing, Hubei Provincial Center for Disease Control and Prevention.

2.5. Aerosol transmission

Fluorescent polystyrene (PS) nanoparticles (100 nm) were used as the virus-mimic nanoparticles to emulate the aerosols containing SARS-CoV-2 virus. An air compressor HP-01 (Tianjin Hengao Technology Development Co., Ltd, China) pressurized PS solution to 18 kPa. 2 mL of PS solution (0.1 mg mL^{-1}) was emitted into a chamber (1.0 L) from the airbrush at 10 L min^{-1}, with a duration of one second every five seconds to produce aerosols contained fluorescent virus-mimic PS nanoparticles. The size distribution of aerosols was measured by a spray laser particle size analyzer Winner 311XP (Jinan Winner Particle Instrument Stock Co., Ltd, China). Each mask or fabric was held tightly with an O-ring over a nozzle (with an inner diameter of 40 mm). A silicon wafer was positioned 1 mm from the mask to collect transmitted aerosols. The aerosols that attached on the silicon wafer and surfaces of masks and household fabrics were detected using a fluorescent microscope (CKX53, Olympus, Tokyo, Japan). A simple white light controller pE-300^{lite} (KOSTER & CoolLED, UK) worked at 70% power for fluorophore excitation. Six images were captured randomly at 10 × magnification per test. The average fluorescence intensity of each image was analyzed via ImageJ software. All raw images were converted to an 8-bit image format. A minimum and maximum contrast threshold was set to 15 and 250, respectively. All experimental conditions and post-processing methods were fixed to reduce error.

3. Results and discussion

3.1. Transformation of standard masks and fabrics to R2A masks

In a typical life circle of R2A mask, 1) the microstructures of standard masks (i.e., disposable and N95 mask) and household fabrics (i.e., cotton and polyester) can be functionalized by a biocompatible and sustainable polyphenol-based functionalization method (Figs. 1a, b and S2) (Guo et al., 2018, 2016, 2014; Luo et al., 2019; Ejima et al., 2013; Zhao et al., 2020; Qiu et al., 2021; Li et al., 2021). The polyphenol-based nano-coating is self-assembled by the coordination between copper ions (Cu^{II}) and catechol/galloyl groups, abundant in plant polyphenols. Such polyphenol-based nanocoatings can function as a shielding layer to capture and deactivate the virus and bacteria carried by air flow/aerosols (Fig. 1c). 2) After the use of mask, at mild acidic condition (such as spraying low concentration of acetic acid solution), the R2A nano-coatings can be disassembled (Lee et al., 2007; Park et al., 2014; Holten-Andersen et al., 2011; Sedó et al., 2013), accompanied with the removal of captured virus and bacteria (Fig. 1d). 3) The used mask can be regenerated by the next-cycle formation of R2A nanocoatings to re-obtain the antiviral, antibacterial, and aerosol rejection properties. In a conventional lifespan of mask, the used mask still possesses infection risk due to the remaining active virus and bacteria on the surface (Fig. 1e). Additionally, due to the lack of regenerability, the disposed masks have caused severe environmental challenges on the land (World Is One News, 2020), in the ocean (Miller, 2020; Giuliani-Hoffman, 2020), and even across the entire ecosystem (Fig. 1f) (Sarcletti et al., 2021; Ragusa et al., 2021; Brahney et al., 2021). Therefore, we rationalized that this assembly-disassembly cycle of polyphenol-based R2A nanocoatings can profoundly resolve the current mask shortage and

relieve the pressure of plastics pollution.

The microstructures of R2A masks showed relatively rough surfaces after the R2A surface functionalization (Figs. S3–S6). The corresponding peaks of the O-C group in X-ray photoelectron spectroscopy (XPS) O 1s spectra (Figs. S7 and S8) and ultraviolet-visible near-infrared diffuse reflection (UV–Vis–NIR DR) spectra (Fig. S9) also confirmed the corresponding surface chemical compositions and supported the assembly-disassembly formation of metal-organic nanocoatings on R2A masks, suggesting their facile regenerability. The R2A nanocoatings also increased the hydrophilicity of the surface of R2A masks corresponding to the reduced water contact angel from 145.3° to 119.6° and the water drop can infiltrate the surface of R2a-disposable mask in 30 s (Fig. S10), which enabled the surfaces of R2A masks with high affinity and deactivation to the virus contained in aerosols (Yu et al., 2021; Huang et al., 2020a,b). Notably, for the enhanced surface hydrophilicity, the air-flowing pressures of R2A masks could be further reduced (Fig. S11), providing an enhanced wearing comfort. Flow cytometry analysis further identified the apoptosis of CHO K1 cells induced by R2A masks. The apoptosis rate and alive rate of incubating CHO K1 cells released from commercial disposable mask are 0.48% and 99.2%, respectively (Fig. S12).

3.2. Imparting inhibition property against SARS-CoV-2

COVID-19 is caused by the highly contagious SARS-CoV-2 virus. Currently, there are no clinically proven therapeutic methods that inhibit the viability of SARS-CoV-2 (Talha, 2021; Deng et al., 2021; Zeng et al., 2021; Kim et al., 2021; Li et al., 2020; Tang et al., 2020, 2021). We tested the antiviral property of R2A nanocoatings against SARS-CoV-2 to exam the potential viral deactivation of these functionally-enhanced masks. The monolayer Vero-E6 cells were formed at the bottom of 12-well plates before performing the plaque assay. SARS-CoV-2 (1.58 × 10^7 TCID50 mL^{-1}) and suspensions of R2A nanocomplexes were mixed and incubated in the 12-well plates. Fig. 2a shows a schematic for the infectious titers of SARS-CoV-2 determined by the plaque assay using Vero-E6 cells, on which the R2A nanocomplexes has a neglected toxic effect after the incubation for 48 h (Fig. S13). Vero-E6 cells were fixed and stained to observe the viral plaque formation. When the inoculum of R2A nanocomplexes remained in the wells throughout the incubation period, the monolayer of Vero-E6 cells appeared to be intact with no obvious formation of viral plaques (Fig. 2b). In contrast, without the inoculum of R2A nanocomplexes, the shapes of Vero-E6 cells showed deformation and a large number of visible plaques could be observed at different viral concentrations. Notably, the experimental groups incubated with R2A nanocomplexes in all four dilutions showed no plaque forming units (PFU) of SARS-CoV-2 (Fig. 2c). These results indicates that R2A nanocoatings on mask have at least 10^5 PFU mL^{-1} inhibitory titer against SARS-CoV-2. On the other hand, the plaques of control group (only inoculum SARS-CoV-2) showed more than 3000 PFU 100 μL^{-1} in the 10^{-1} dilution group.

The cytopathic effect (CPE) assay was also performed in Vero-E6 cells induced by SARS-CoV-2 infection (Fig. 2d). SARS-CoV-2 (1.58 × 10^7 TCID50 mL^{-1}) was mixed with R2A nanocomplexes at the equal volume and further diluted into different concentrations with Dulbecco's modified Eagle medium (DMEM) containing FBS. An appropriate dilution of each gradient was added to the corresponding wells with Vero-E6 cells and the mixtures were incubated to observe the CPE. The control group (without R2A nanocomplexes) was set at the same time. Our results showed that Vero-E6 cells in all five virus titer groups containing R2A nanocomplexes grew normally without producing any CPE, even in the highest viral concentration group (5000 TCID50 100 μL^{-1}) (Fig. 2e). These experimental results indicated that SARS-CoV-2 could be significantly inactivated with no proliferation, indicating a highly effective inhibition of R2A nanocomplexes on SARS-CoV-2. In the control group (without R2A nanocomplexes), after the infection and incubation of SARS-CoV-2, a typical CPE could be observed in each of the
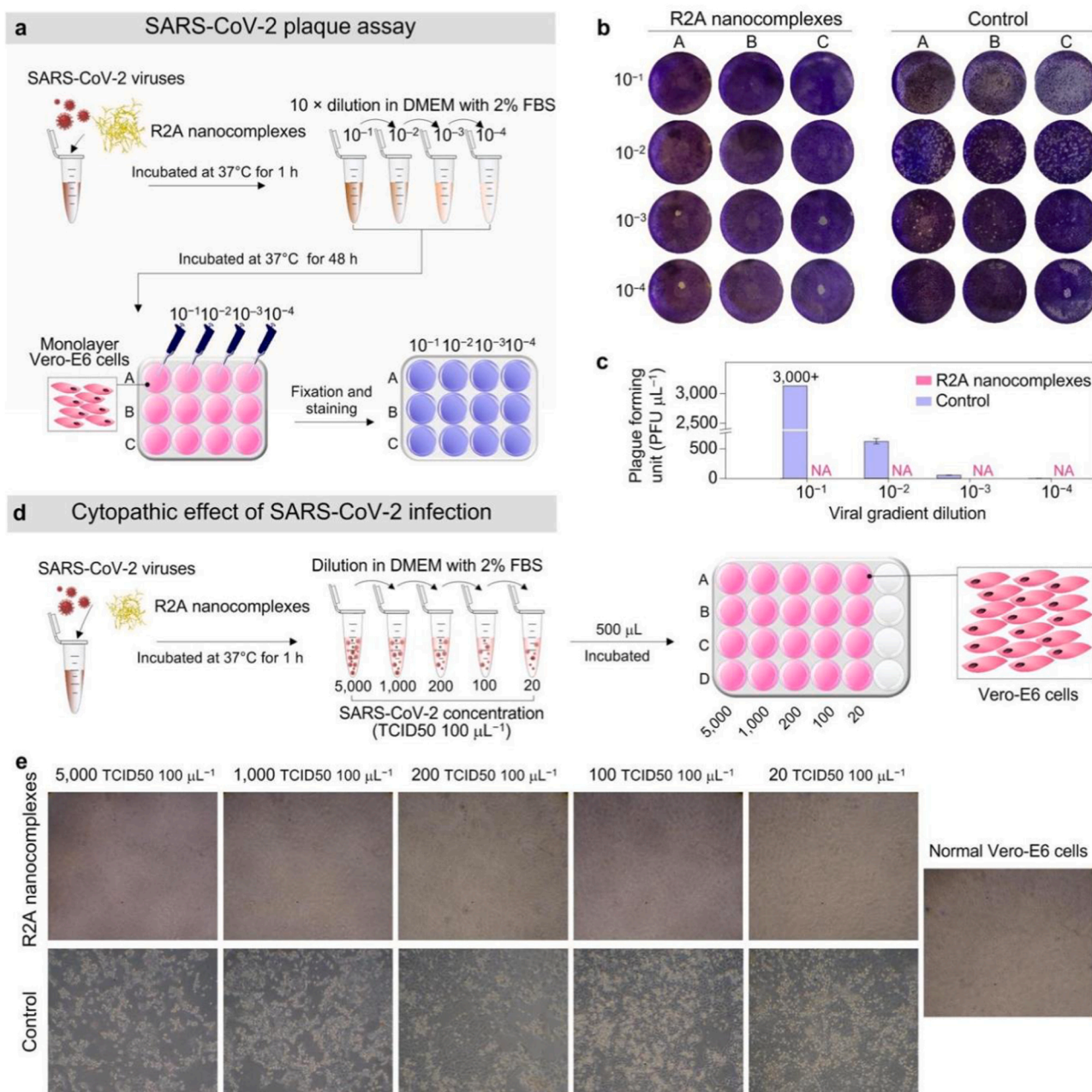
Fig. 2. Antiviral assay procedures of R2A nanocoatings against SARS-CoV-2. (a) Schematic illustration of SARS-CoV-2 plaque assay for Vero-E6 cells with R2A nanocomplexes. (b) Optical plaque photographs of SARS-CoV-2 with different titer gradients in a 12-well plate for Vero-E6 cells with/without R2A nanocomplexes after fixation and staining. The white plagues in panels were caused by the culture media loss after washing. (c) Statistical PFU of SARS-CoV-2 with different titer gradients for Vero-E6 cells with/without R2A nanocomplexes. (d) Schematic illustration of CPE assay of SARS-CoV-2 on Vero-E6 cells. (e) Optical CPE photographs of SARS-CoV-2 in different concentrations (5000, 1000, 200, 100, 20 TCID50 100 μL^{-1}) and normal Vero-E6 cells after incubation. The microscope magnifications were 20×. Error bars in c represent the standard deviation from triplicate experiments.

above five titer gradients (5000, 1000, 200, 100, and 20 TCID50 100 μL^{-1}). These results indicated that R2A nanocomplexes and corresponding nanocoatings on masks could effectively inhibit the infection induced by SARS-CoV-2 to Vero-E6 cells, likely due to the combinational effects of polyphenols and copper ions released from the R2A nanocoatings, in which natural polyphenols could inhibit virus protein expressions and copper ions could generate ROS-mediated viral prevention of replication and RNA degradation (Imani et al., 2020; Zhu et al., 2020; Li et al., 2021).

3.3. Regenerative aerosol filtering property

Respiratory particles, including aerosol particles and larger droplets, can carry viruses and are often used to visualize the transmission of airborne viruses (Cheng et al., 2021; Bourouiba, 2020). Fig. 3a shows a schematic of human respiratory processes and aerosol filtering test of R2A mask. Fluorescent polystyrene nanoparticles with the size of 100 nm were used to just mimic the size and shape of airborne viruses (Fig. 3b) (Prather et al., 2020; Lustig et al., 2020). Fig. 3c shows that after the filtration by masks, the outer layer of original disposable mask contained a high density of droplets due to its inherent hydrophobicity, preventing the aerosol particles to infiltrate. But owing to the inherent
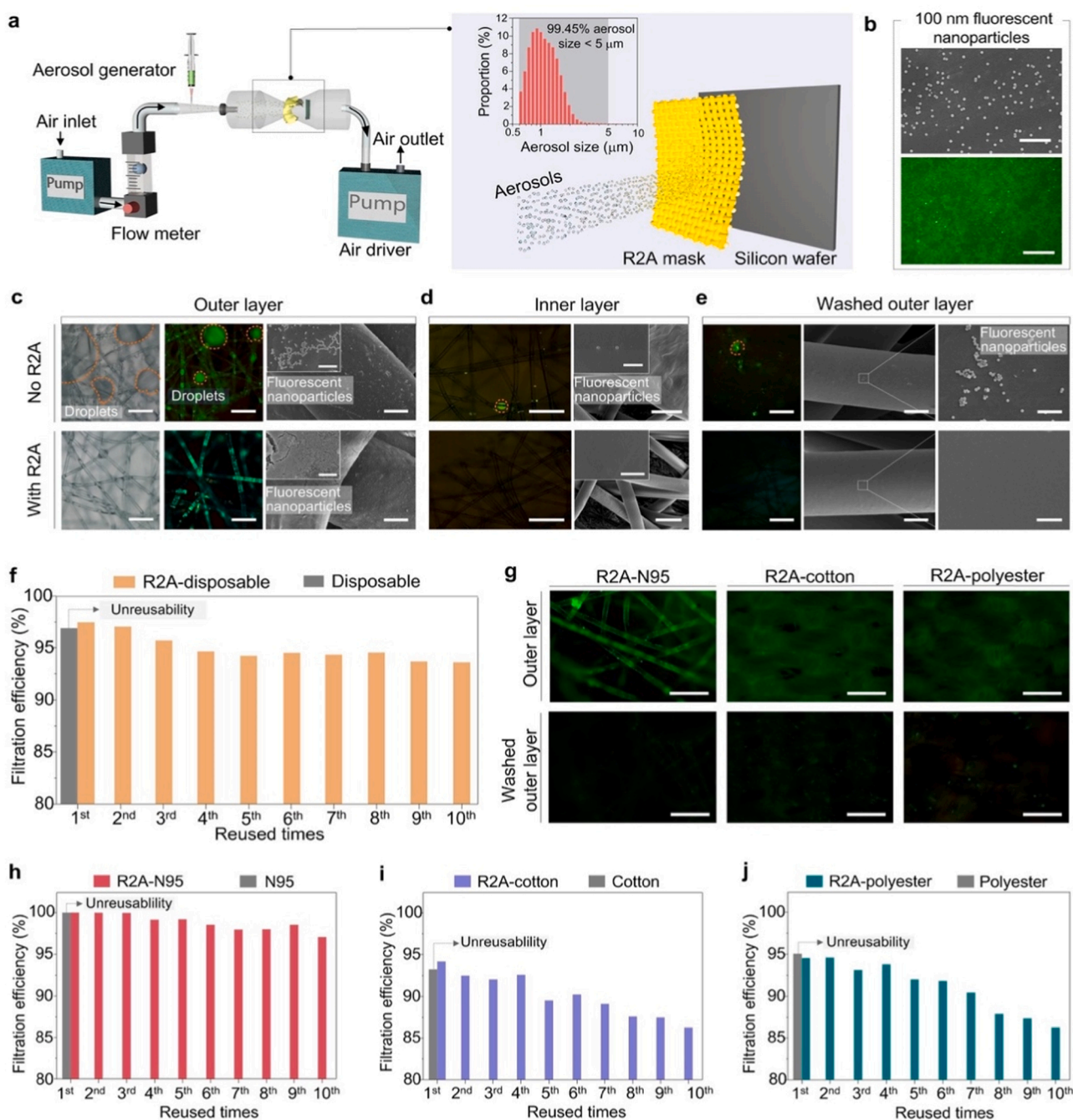
Fig. 3. Regenerative protection of R2A masks from aerosols containing virus-mimic nanoparticles. (a) Schematic of aerosol generation apparatus and pulsed aerosols containing fluorescent, virus-mimic PS nanoparticles (100 nm) passing through R2A masks by steady-state, and forced convection air flux. Inset is the size distribution of aerosols generated by our apparatus. (b) SEM images and fluorescent photographs of fluorescent PS nanoparticles on silicon wafer. (c–e) Representative fluorescent and SEM images of the outer layers and inner layers of disposable and R2A-disposable mask before and after washing. (f) Aerosols rejection performances comparison between disposable mask and corresponding R2A-disposable mask in a 10-cycle test. (g) Representative fluorescent photographs of the outer layers of R2A-N95, R2A-cotton, and R2A-polyester masks before and after washing. (h–j) Simulated aerosols rejection performances comparison between N95 mask/household fabrics (cotton and polyester) and corresponding R2A masks in a 10-cycle test. Scale bars, 2 μm (SEM images), 100 μm (fluorescent photographs).

hydrophilicity, the aerosol particles can the soak outer layer surface of R2A-disposable mask delivering into high fluorescence signal of fibrous surface. SEM images show that fluorescent virus-mimic nanoparticles are adhered on the outer fibrous surface of R2A-disposable mask. Additionally, the inner layer of disposable mask also shows the fluorescence signal of virus-mimic nanoparticles, indicating the penetration of aerosols throughout the layers of disposable mask (Fig. 3d). However, the inner layer of R2A-disposable mask has no fluorescence signal, supporting its efficient aerosol rejection capability.

After washing and removal of R2A nanocoatings on mask, the surface layer of R2A-disposable mask shows no fluorescence and presents smooth surface (Fig. 3e), supporting the removal of virus-mimic nanoparticles with the disassembly of R2A nanocoatings. In contrast, fluorescence signal of virus-mimic nanoparticles can be observed on the surface of disposable mask even after washing by the Milli-Q water. The corresponding initial filtering efficiency of R2A-disposable mask for aerosols is ~ 97.50% and can be maintained over ~ 93.62% after 10 cycles (Fig. 3f).

Similarly, the outer layers of R2A-N95, R2A-cotton, and R2A-polyester masks also showed fluorescence after filtration (Fig. 3g), while no signal of fluorescence could be found on the inner layers (Figs. S14–S16) and corresponding silicon wafers (Fig. S17). After washing, virus-mimic nanoparticles can be removed from the outer layers (Figs. 3g and S18–S20). In contrast, the virus-mimic nanoparticles on the outer layers of pristine N95 mask, cotton matrix, and polyester matrix are still observed (Figs. S21–S23). Remarkably, the aerosol filtration efficiency of regenerated R2A-N95 mask still maintained over 96% after 10-time cycles (Fig. 3h–j). Collectively, R2A masks provide an effective protection against respiratory infections by the enhanced

aerosol filtering property to break the chain of transmission through saliva and droplets exhaled from infected people.

3.4. Regenerative antibacterial property

Imparting antibacterial property to standard masks can provide an additional measure for the prevention of bacteria-caused respiratory diseases and common bacterial skin infection (e.g., intertrigo). We tested the antibacterial property and regenerability of R2A masks. R2A masks were incubated with *Escherichia coli* (*E. coli*) suspensions, and then rinsed by sterilized saline solution to release the bacteria from mask
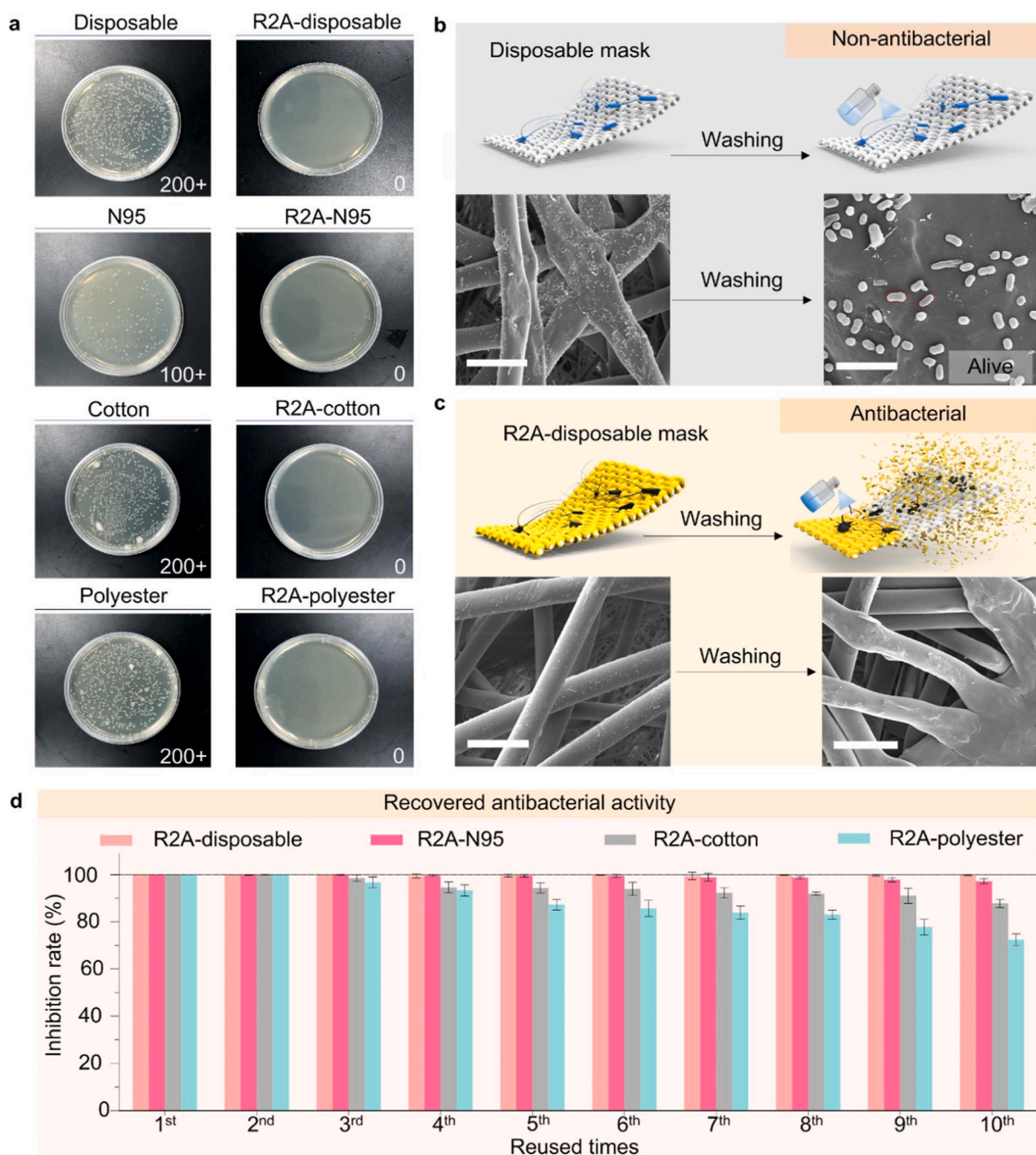

Fig. 4. Antibacterial property and regenerable stability of R2A masks. (a) Optical photo images of *E. coli* colonies cultured on petri dish. (b, c) Schematic illustration of non-antibacterial and antibacterial abilities of the standard masks, household fabrics, and R2A masks. Insets are SEM images of bacteria on disposable and R2A-disposable mask before and after washing. Scale bars, 50 μm (before) and 10 μm (after). (d) Antibacterial performances of R2A masks in a 10-cycle test. Error bars in (d) represent the standard deviation from triplicate experiments.

surfaces. The collected bacteria were measured by colony forming units (CFU). Figs. 4a and S24 show a significant number of colonies in the control groups (without R2A nanocoatings). In contrast, no bacterial growth can be observed in the groups incubated with R2A masks. SEM images also show a significant number of flourished bacteria on the surface of disposable mask after 12 h incubation even after rinsing, suggesting its negligible inhibition, which provides an evidence on the infectious risk of normal masks whether during or after use (Fig. 4b). Whereas, the surface of R2A-disposable mask shows no intact bacteria,

demonstrating the contact-killing ability of R2A nanocoatings (Fig. 4c). After washing by the mild acid solution, the R2A nanocoatings and attached bacteria debris could be removed with the disassembly of the R2A nanocoatings. Similar antibacterial performances are also observed in the R2A-N95, R2A-cotton, and R2A-polyester masks (Figs. S25–S27).

Our experimental results show that R2A-disposable mask exhibits ~ 99% antibacterial efficacy to *E. coli* stain (Fig. 4d). Moreover, the regenerated R2A-disposable mask can maintain the inhibition rate over 98% after 10-time cycles. The function-enhanced R2A-N95, R2A-cotton,
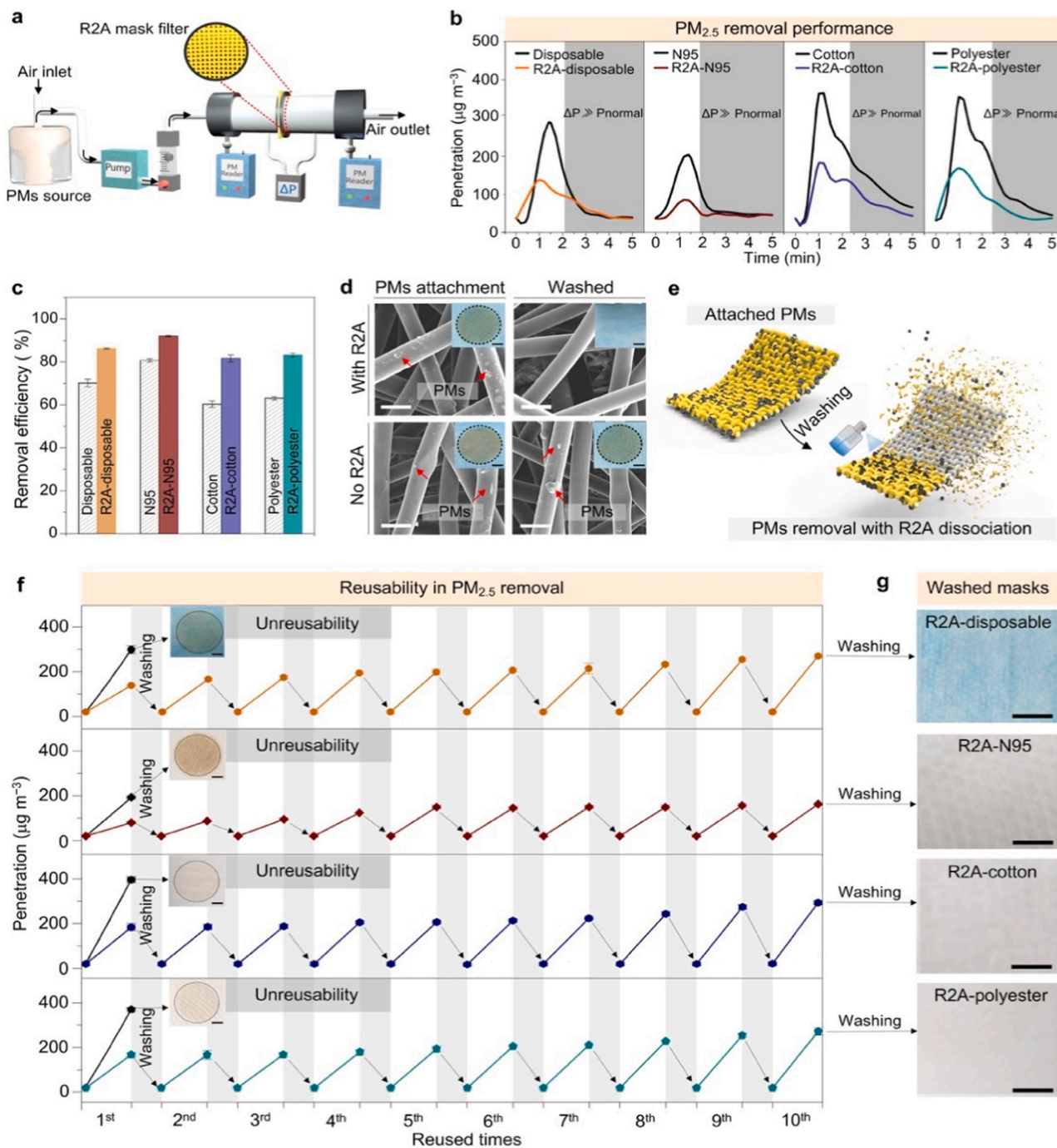

Fig. 5. Filtration performances of R2A masks in the protection from PMs pollution. (a) Schematic of PMs generation apparatus. (b,c) PM$_{2.5}$ removal efficiencies of R2A masks in 5 min (d) SEM images and digital photographs (insets) of PMs trapped on the outer layer of disposable mask and R2A-disposable mask before and after washing. (e) Schematic illustration of PMs removal with disassembly of R2A nanocoatings. (f) PM$_{2.5}$ filtration performances of R2A masks in a 10-cycle test. Insets are the digital photographs of un-reusable standard masks and household fabrics after the PMs filtration. (g) The digital photographs of washed R2A masks after a 10-cycle test. Each filtration test was performed for 5 min and the initial concentration of PMs was higher than 1000 μg m^{-3}. Scale bars, 25 μm (SEM images), 0.5 cm (insets of d and f, and photographs of g). Error bars in **c** and **f** represent the standard deviation from triplicate experiments.

and R2A-polyester masks all present highly efficient antibacterial performances during the regeneration experiments. In addition, the R2A masks still exhibit stable antibacterial performances after weathering tests (Figs. S28 and S29). SEM images profiled the intact fibrous microstructures of the R2A masks even after bended 10,000 times (Figs. S30–S33), suggesting the comfortability of R2A nanocoatings to withstand the mechanical stress.

3.5. Filtration performance for particulate matters

Ambient particulate matters (PMs) are linked to several health risks in high-, low-, and middle-income countries due to their evidence-supported threats to the human respiratory system (Nel, 2005). We further investigated the functionalization of masks with R2A nanocoatings for enhancing the filtration property against PMs. The PMs filtration performances of different R2A masks were tested by the in-house designed testing device (Fig. 5a) (Liu et al., 2015). Compared with original masks and fabrics, the corresponding R2A masks perform high $PM_{2.5}$ filtration efficiencies (Fig. 5b, c), probably due to the formation of multiple interactions between mask surfaces and particles (Ejima et al., 2013; Guo et al., 2014). Additionally, R2A masks also present high filtration performances of PM_{10} and $PM_{1.0}$ (Figs. S34 and S35). SEM images show that the PMs can be effectively captured on the surfaces of R2A masks, which is also reflected from the color change from light blue to yellow-brown in the photographic images (Fig. 5d). After washing by mild acid solution, the surface color of R2A-disposable mask changed from yellow-brown to native color, due to the disassembly of R2A nanocoatings and removal of attached PMs (Fig. 5e). Whereas, attached PMs cannot be removed from the surfaces of pristine masks simply by washing, as evidenced by the SEM images and photographic images. Similarly, the captured PMs on R2A-N95, R2A-cotton, and R2A-polyester masks can be also removed by simple washing processes (Figs. S36–S38), while the pristine masks and fabrics without R2A nanocoatings cannot be regenerated after the filtration of PMs.

In the recycling tests, the $PM_{2.5}$ concentration after filtration by R2A-disposable mask was remained at a low level (138 μg m^{-3}) (the value of disposable mask, 298 μg m^{-3}), with the removal efficiency of 86.20% (disposable mask, 70.17%) (Fig. 5f). When R2A-disposable mask was washed and R2A nanocoatings were rebuilt, the regenerated R2A-disposable mask still showed a high removal efficiency for $PM_{2.5}$ over 83.40%, which could be maintained in the subsequent 10-time cycles. For the smaller and larger PMs ($PM_{1.0}$ and PM_{10}), its removal efficiencies could be also maintained at ~ 84.00% and ~ 61.00% throughout 10-time cycles, respectively (Fig. S39). Similar results can be obtained by other types of R2A masks for PMs with different sizes (Figs. S40–S42).

4. Conclusions

We developed a facile and sustainable strategy to impart multifunctional properties (reusable, antiviral, and antibacterial, referred to as R2A, to commonly-used standard masks and household fabrics through an easy, rapid, low-cost surface functionalization method based on the biomass resource of natural polyphenols. The functionally-enhanced R2A masks provide an effective protection against respiratory diseases by inhibiting the activity of SARS-CoV-2 virus and model bacteria. These multifunctional properties can be maintained for long-term usage through a circular assembly-disassembly formation of R2A nanocoatings. The disassembly of the nanocoatings in a mild acidic condition can remove the contaminants (including bacteria debris, virus debris, and microparticles) on the surfaces of masks. Taken together, this simple functional enhancement strategy of masks is of immediate importance to mitigate the current COVID-19 pandemic and future respiratory diseases, as well as to address worldwide plastic pollution from the non-cyclic use of non-regenerative masks.

CRediT authorship contribution statement

Xiaoling Wang: Investigation, Methodology, Supervision, Writing – original draft, Writing – review & editing, Funding acquisition. **Ting Hu:** Investigation, Methodology. **Bing Hu:** Investigation, Methodology. **Yan Liu:** Investigation, Methodology. **Yan Li:** Investigation, Methodology. **Yu Wang:** Writing – review & editing. **Yunxiang He:** Writing – review & editing. **Kun Cai:** Writing – review & editing. **Xingcai Zhang:** Conceptualization, Writing – review & editing, Supervision, Funding acquisition. **Junling Guo:** Conceptualization, Writing – review & editing, Supervision, Funding acquisition.

Declaration of Competing Interest

J.G., X.W., Y.W., and T.H. are inventors on patent application submitted by Sichuan University that covers regenerative, antiviral, and antibacterial mask engineered by polyphenol-based coating described in this paper. J.G. and X.W. declare that they are shareholders of Thinkcloud Biotech, which is developing antibacterial and antiviral products. X.Z., Y.L., B.H., and K.C. declare no competing interests.

Acknowledgments

Author contributions

J.G., X.Z., and X.W. conceived and supervised the research. X.W., Y.L., T.H., and Y.W. designed the experiments and collected the data of antibacterial, reusable, and PMs filtration performance of R2A masks. B.H., Y.L., and K.C. performed the antiviral experiments and co-analysed the results. X.Z., X.W., and T.H. wrote the paper.

Appendix A. Supplementary material

Supplementary data associated with this article can be found in the online version at doi:10.1016/j.jhazmat.2022.128441.

References

Bourouiba, L., 2020. Turbulent gas clouds and respiratory pathogen emissions: potential implications for reducing transmission of COVID-19. J. Am. Med. Assoc. 323, 1837–1838. https://doi.org/10.1001/jama.2020.4756.

Brahney, J., Mahowald, N., Prank, M., Cornwell, G., Klimont, Z., Matsui, H., Prather, K. A., 2021. Constraining the atmospheric limb of the plastic cycle. Proc. Natl. Acad. Sci. USA 118, e2020719118. https://doi.org/10.1073/pnas.2020719118.

Brosseau, L., Ann, R.B., 2009. N95 Respirators and Surgical Masks. NIOSH Science Blog. ⟨https://blogs.cdc.gov/niosh-science-blog/2009/10/14/n95⟩. (Accessed 14 October 2009).

Chen, S., Zhang, S., Galluzzi, M., Li, F., Zhang, X.C., Yang, X.H., Liu, X.Y., Cai, X.H., Zhu, X.L., Li, J.N., Huang, P., 2019. Insight into multifunctional polyester fabrics finished by one-step eco-friendly strategy. Chem. Eng. J. 358, 634–642. https://doi.org/10.1016/j.cej.2018.10.070.

Cheng, Y., Ma, N., Witt, C., Rapp, S., Wild, P.S., Andreae, M.O., Pöschl, U., Su, H., 2021. Face masks effectively limit the probability of SARS-CoV-2 transmission. Science 372, 1439–1443. https://doi.org/10.1038/s41467-021-24115-7.

Chu, D.K., Akl, E.A., Duda, S., Solo, K., Yaacoub, S., Schünemann, H.J., 2020. Face masks, and eye protection to prevent person-to-person transmission of SARS-CoV-2 and COVID-19: a systematic review and meta-analysis. Lancet 395, 1973–1987. https://doi.org/10.1016/S0140-6736(20)31142-9.

Chua, M.H., Cheng, W.R., Goh, S.S., Kong, J.H., Li, B., Lim, J.Y.C., Mao, L., Wang, S.X., Xue, K., Yang, L., Ye, E.Y., Zhang, K.Y., Cheong, W.C.D., Tan, B.H., Li, Z.B., Tan, B. H., Loh, X.J., 2020. Face masks in the new COVID-19 normal: materials, testing, and perspectives. Research, 7286735. https://doi.org/10.34133/2020/7286735.

Current World Population, 2020. ⟨https://www.worldometers.info/world-population-r ef-1⟩. (Accessed 2020).

Deng, X.D., Garcia-Knight, M.A., Khalid, M.M., Servellita, V., Wang, C., Morris, M.K., Sotomayor-González, A., Glasner, D.R., Reyes, K.R., Gliwa, A.S., Reddy, N.P., Martin, C.S.S., Federman, S., Cheng, J., Balcerek, J., Taylor, J., Streithorst, J.A., Miller, S., Sreekumar, B., Chen, P.Y., Schulze-Gahmen, U., Taha, T.Y., Hayashi, J.M., Simoneau, C.R., Kumar, G.R., McMahon, S., Lidsky, P.V., Xiao, Y.H., Hemarajata, P., Green, N.M., Espinosa, A., Kath, C., Haw, M., Bell, J., Hacker, J.K., Hanson, C., Wadford, D.A., Anaya, C., Ferguson, D., Frankino, P.A., Shivram, H., Lareau, L.F., Wyman, S.K., Ott, M., Andino, R., Chiu, C.Y., 2021. Transmission, infectivity, and neutralization of a spike L452R SARS-CoV-2 variant. Cell 184, 3426–3437. https:// doi.org/10.1016/j.cell.2021.04.025.

Ejima, H., Richardson, J.J., Liang, K., Best, J.P., van Koeverden, M.P., Such, G.K., Cui, J. W., Caruso, F., 2013. One-step assembly of coordination complexes for versatile film and particle engineering. Science 341, 154–157. https://doi.org/10.1126/ science.1237265.

Fadare, O.O., Okoffo, E.D., 2020. COVID-19 face masks: a potential source of microplastic fibers in the environment. Sci. Total Environ. 737, 140279 https://doi. org/10.1016/j.scitotenv.2020.140279.

Giuliani-Hoffman, F., 2020. Conservationists Warn COVID Waste May Result in More Masks than Jellyfish in the Sea. ⟨https://cbs58.com/news/conservationists-warn-covid-waste-may-result-in-more-masks-than-jellyfish-in-the-sea⟩. (Accessed 24 June 2020).

Guo, J.L., Ping, Y., Ejima, H., Alt, K., Meissner, M., Richardson, J.J., Yan, Y., Peter, K., von Elverfeldt, D., Hagemeyer, C.E., Caruso, F., 2014. Engineering multifunctional capsules through the assembly of metal-phenolic networks. Angew. Chem. Int. Ed. 53, 5546–5551. https://doi.org/10.1002/anie.201311136.

Guo, J.L., Tardy, B.L., Christofferson, A.J., Dai, Y.L., Richardson, J.J., Zhu, W., Hu, M., Ju, Y., Cui, J.W., Dagastine, R.R., Yarovsky, I., Caruso, F., 2016. Modular assembly of superstructures from polyphenol-functionalized building blocks. Nat. Nanotechnol. 11, 1105–1111. https://doi.org/10.1038/nnano.2016.172.

Guo, J.L., Suástegui, M., Sakimoto, K.K., Moody, V.M., Xiao, G., Nocera, D.G., Joshi, N.S., 2018. Light-driven fine chemical production in yeast biohybrids. Science 362, 813–816. https://doi.org/10.1126/science.aat9777.

Holten-Andersen, N., Harrington, M.J., Birkedal, H., Lee, B.P., Messersmith, P.B., Yee, K., Lee, G., Waite, J.H., 2011. pH-induced metal-ligand cross-links inspired by mussel yield self-healing polymer networks with near-covalent elastic moduli. Proc. Natl. Acad. Sci. USA 108, 2651–2655. https://doi.org/10.1073/pnas.1015862108.

Howard, J., Huang, A., Li, Z.Y., Tufekci, Z., Zdimal, V., Van der Westhuizen, H., von Delft, A., Price, A., Fradman, L., Tang, L.H., Tang, V., Waston, G.L., Bax, C.E., Shaikh, R., Questier, F., Hernandez, D., Chu, L.F., Ramirez, C.M., Rimoin, A.W., 2021. An evidence review of face masks against COVID-19. Proc. Natl. Acad. Sci. USA 118, 4. https://doi.org/10.1073/pnas.2014564118.

Huang, H.Y., Park, H., Liu, Y.H., Huang, J.X., 2020a. On-mask chemical modulation of respiratory droplets. Matter 3, 1791–1810. https://doi.org/10.1016/j. matt.2020.10.012.

Huang, L.B., Xu, S.Y., Wang, Z.Y., Xue, K., Su, J.J., Song, Y., Chen, S.J., Zhu, C.L., Tang, B.Z., Ye, R.Q., 2020b. Self-reporting and photothermally enhanced rapid bacterial killing on a laser-induced graphene mask. ACS Nano 14, 12045–12053. https://doi.org/10.1021/acsnano.0c05330.

Imani, S.M., Ladouceur, L., Marshall, T., Maclachlan, R., Soleymani, L., Didar, T.F., 2020. Antimicrobial nanomaterials and coatings: current mechanisms and future perspectives to control the spread of viruses including SARS-CoV-2. ACS Nano 14, 12341–12369. https://doi.org/10.1021/acsnano.0c05937.

Kim, J.H., Marks, F., Clemens, J.D., 2021. Looking beyond COVID-19 vaccine phase 3 trials. Nat. Med. 27, 205–211. https://doi.org/10.1038/s41591-021-01230-y.

Kumar, S., Karmacharya, M., Joshi, S.R., Gulenko, O., Park, J., Kim, G.H., Cho, Y.K., 2020. Photoactive antiviral face mask with self-sterilization and reusability. Nano Lett. 21, 337–343. https://doi.org/10.1021/acs.nanolett.0c03725.

Lee, H., Dellatore, S.M., Miller, W.M., Messersmith, P.B., 2007. Mussel-inspired surface chemistry for multifunctional coatings. Science 318, 426–430. https://doi.org/ 10.1126/science.1147241.

Leung, C.C., Lam, T.H., Cheng, K.K., 2020a. Mass masking in the COVID-19 epidemic: people need guidance. Lancet 395, 945. https://doi.org/10.1016/S0140-6736(20) 30520-1.

Leung, N.H.L., Chu, D.K.W., Shiu, E.Y.C., Chan, K.H., McDevitt, J.J., Hau, B.J.P., Yen, H. L., Li, Y., Ip, D.K.M., Malik Peiris, J.S., Seto, W.H., Leung, G.M., Milton, D.K., Cowling, B.J., 2020b. Respiratory virus shedding in exhaled breath and efficacy of face masks. Nat. Med. 26, 676–680. https://doi.org/10.1038/s41591-020-0843-2.

Li, J., Li, J.Y., Wei, J.Y., Zhu, X.B., Qiu, S.H., Zhao, H.C., 2021. Copper tannic acid-coordinated metal-organic nanosheets for synergistic antimicrobial and antifouling coatings. ACS Appl. Mater. Interfaces 13, 10446–10456. https://doi.org/10.1021/ acsami.0c22321.

Li, K.N., Huang, B., Wu, M., Zhong, A.F., Li, L., Cai, Y., Wang, Z.H., Wu, L.X., Zhu, M.Y., Li, J., Wang, Z.Y., Wu, W., Li, W.L., Bosco, B., Gan, Z.H., Qiao, Q.H., Wu, J., Wang, Q.H., Wang, S.K., Xia, X.Y., 2020. Dynamic changes in anti-SARS-CoV-2 antibodies during SARS-CoV-2 infection and recovery from COVID-19. Nat. Commun. 11, 6044. https://doi.org/10.1038/s41467-020-19943-y.

Li, P., Li, J.Z., Feng, X., Li, J., Hao, Y.C., Zhang, J.W., Wang, H., Yin, A.X., Zhou, J.W., Ma, X.J., Wang, B., 2019. Metal-organic frameworks with photocatalytic bactericidal activity for integrated air cleaning. Nat. Commun. 10, 1–10. https://doi.org/ 10.1038/s41467-019-10218-9.

Liu, C., Hsu, P.C., Lee, H.W., Ye, M., Zheng, G.Y., Liu, N., Li, W.Y., Cui, Y., 2015. Transparent air filter for high-efficiency $PM_{2.5}$ capture. Nat. Commun. 6, 1–9. https://doi.org/10.1038/ncomms7205.

Luo, W., Xiao, G., Tian, F., Richardson, J.J., Wang, Y.P., Zhou, J.F., Guo, J.L., Liao, X.P., Shi, B., 2019. Engineering robust metal-phenolic network membranes for uranium extraction from seawater. Energy Environ. Sci. 12, 607–614. https://doi.org/ 10.1039/C8EE01438H.

Lustig, S.R., Biswakarma, J.J.H., Rana, D., Tilford, S.H., Hu, W.K., Su, M., Rosenblatt, M. S., 2020. Effectiveness of common fabrics to block aqueous aerosols of COVID virus-mimic nanoparticles. ACS Nano 14, 7651–7658. https://doi.org/10.1021/ acsnano.0c03972.

Miller, R.W., 2020. More Masks than Jellyfish: Environmental Groups Worry about Coronavirus Waste in Oceans. ⟨https://www.coloradoan.com/story/news/nation/ 2020/06/09/coronavirus-waste-oceans-masks-gloves-raises-environmental-concer n/5325194002/⟩. (Accessed 9 June 2020).

Nel, A., 2005. Air pollution-related illness: effects of particles. Science 308, 804–806. https://doi.org/10.1126/science.1108752.

Park, J.H., Kim, K., Lee, J., Choi, J.Y., Hong, D., Yang, S.H., Caruso, F., Lee, Y., Choi, I.S., 2014. A cytoprotective and degradable metal-polyphenol nanoshell for single-cell encapsulation. Angew. Chem. Int. Ed. 53, 12420–12425. https://doi.org/10.1002/ anie.201405905.

Prata, J.C., Silva, A.L.P., Walker, T.R., Duarte, A.C., Rocha-Santos, T., 2020. COVID-19 pandemic repercussions on the use and management of plastics. Environ. Sci. Technol. 54, 7760–7765. https://doi.org/10.1021/acs.est.0c02178.

Prather, K.A., Wang, C.C., Schooley, R.T., 2020. Reducing transmission of SARS-CoV-2. Science 368, 1422–1424. https://doi.org/10.1126/science.abc6197.

Qiu, X.L., Wang, X.L., He, Y.X., Liang, J.Y., Liang, K., Tardy, B.L., Richardson, J.J., Hu, M., Wu, H., Zhang, Y., Rojas, O.J., Manners, I., Guo, J.L., 2021. Superstructured mesocrystals through multiple inherent molecular interactions for highly reversible sodium ion batteries. Sci. Adv. 7 https://doi.org/10.1126/sciadv.abh3482 eabh3482.

Ragusa, A., Svelato, A., Santacroce, C., Catalano, P., Notarstefano, V., Carnevali, O., Papa, F., Rongioletti, M.C.A., Baiocco, F., Draghi, S., D'Amore, E., Rinaldo, D., Matta, M., Giorgini, E., 2021. Plasticenta: first evidence of microplastics in human placenta. Environ. Int. 146, 106274 https://doi.org/10.1016/j.envint.2020.106274.

Ranney, M.L., Griffeth, V., Jha, A.K., 2020. Critical supply shortages—the need for ventilators and personal protective equipment during the COVID-19 pandemic. N. Engl. J. Med. e41, 382. https://doi.org/10.1056/NEJMp2006141.

Sarcletti, M., Park, H., Wirth, J., Englisch, S., Eigen, A., Drobek, D., Vivod, D., Friedrich, B., Tietze, R., Alexiou, C., Zahn, D., Zubiri, B.A., Spiecker, E., Halik, M., 2021. The remediation of nano-/microplastics from water. Mater. Today. https:// doi.org/10.1016/j.mattod.2021.02.020.

Sedó, J., Saiz-Poseu, J., Busqué, F., Ruiz-Molina, D., 2013. Catechol-based biomimetic functional materials. Adv. Mater. 25, 653–701. https://doi.org/10.1002/ adma.201202343.

Stanford, M.G., Li, J.T., Chen, Y., McHugh, E.A., Liopo, A., Xiao, H., Tour, J.M., 2019. Self-sterilizing laser-induced graphene bacterial air filter. ACS Nano 13, 11912–11920. https://doi.org/10.1021/acsnano.9b05983.

Talha, B., 2021. Understanding variants of SARS-CoV-2. Lancet 397, 462. https://doi. org/10.1016/S0140-6736(21)00298-1.

Tang, Z., Zhang, X.C., Shu, Y.Q., Guo, M., Zhang, H., Tao, W., 2021. Insights from nanotechnology in COVID-19 treatment. Nano Today 36, 101019. https://doi.org/ 10.1016/j.nantod.2020.101019.

Tang, Z.M., Kong, N., Zhang, X.C., Liu, Y., Hu, P., Mou, S., Liljeström, P., Shi, J.L., Tan, W.H., Kim, S.J., Cao, Y.H., Langer, R., Leong, K.W., Farokhzad, O.C., Tao, W., 2020. A materials-science perspective on tackling COVID-19. Nat. Rev. Mater. 5, 847–860. https://doi.org/10.1038/s41578-020-00247-y.

United Nations Environment Programme, 2020. Waste Management During the COVID-19 Pandemic. ⟨https://www.unep.org/resources/report/waste-management-duri ng-covid-19-pandemic-response-recovery⟩. (Accessed 12 August 2020).

Wang, C.C., Prather, K.A., Sznitman, J., Jimenez, J., Lakdawala, S.S., Tufekci, Z., Marr, L. C., 2021. Airborne transmission of respiratory viruses. Science 373. https://doi.org/ 10.1126/science.abd9149 eabd9149.

World Health Organization, 2020. Shortage of Personal Protective Equipment Endangering Health Workers Worldwide. ⟨https://www.who.int/news-room/detai l/03-03-2020-shortage-of-personal-protective-equipment-endangering-health-worke rs-worldwide⟩. (Accessed 3 March 2020).

World Is One News, 2020. Monkeys in a Finnish Zoo Preferred Noise of Traffic over Nature, Ongoing Study Finds. ⟨https://www.wionews.com/world/monkeys-in-a-finnish-zoo-preferred-noise-of-traffic-over-nature-ongoing-study-finds-342200⟩. (Accessed 10 November 2020).

World Wildlife Fund, 2020. In the Disposal of Masks and Gloves, Responsibility Is Required. ⟨https://www.wwf.it/scuole/?53500%2FNello-smaltimento-di-mascheri ne-e-guanti-serve-responsabilita⟩. (Accessed 29 April 2020).

Yu, Z.L., Kadir, M., Liu, Y.H., Huang, J.X., 2021. Droplet-capturing coatings on environmental surfaces based on cosmetic ingredients. Chem 7, 1–11. https://doi. org/10.1016/j.chempr.2021.05.017.

Zeng, C.X., Hou, X.C., Bohmer, M., Dong, Y.Z., 2021. Advances of nanomaterials-based strategies for fighting against COVID-19. View. https://doi.org/10.1002/ VIW.20200180, 20200180.

Zhang, G.H., Zhu, Q.H., Zhang, L., Yong, F., Zhang, Z., Wang, S.L., Wang, Y., He, L., Tao, G.H., 2020. High-performance particulate matter including nanoscale particle removal by a self-powered air filter. Nat. Commun. 11, 1–10. https://doi.org/ 10.1038/s41467-020-15502-7.

Zhao, Z.M., Pan, D.C., Qi, Q.M., Kim, J., Kapate, N., Sun, T., Wyatt Shields IV, C., Wang, L.L.W., Wu, D., Kwon, C.J., He, W., Guo, J.L., Mitragotri, S., 2020.

Engineering of living cells with polyphenol-functionalized biologically active nanocomplexes. Adv. Mater. 32, 2003492 https://doi.org/10.1002/adma.202003492.

Zhong, H., Zhu, Z.R., Lin, J., Cheung, C.F., Lu, V.L., Yan, F., Chan, C.Y., Li, G.J., 2020. Reusable and recyclable graphene masks with outstanding superhydrophobic and photothermal performances. ACS Nano 14, 6213–6221. https://doi.org/10.1021/acsnano.0c02250.

Zhu, N., Wang, W.L., Liu, Z.D., Liang, C.Y., Wang, W., Ye, F., Huang, B.Y., Zhao, L., Wang, H.J., Zhou, W.M., Deng, Y., Mao, L.F., Su, C.Y., Qiang, G.L., Jiang, T.J., Zhao, J.C., Wu, G.Z., Song, J.D., Tan, W.J., 2020. Morphogenesis and cytopathic effect of SARS-CoV-2 infection in human airway epithelial cells. Nat. Commun. 11, 1–8. https://doi.org/10.1038/s41467-020-17796-z.